Processing and characterization of geopolymer and sintered geopolymer foams of waste glass powders

Dilan Polat, Mustafa Güden [*]

Department of Mechanical Engineering, Izmir Institute of Technology, Gülbahçe Köyü, Urla, Izmir, Turkey

ABSTRACT

Geopolymer foams of fine and coarse waste glass (WG) powders were prepared using an activation solution of NaOH (8 M) and Na_2SiO_3. The effects of WG powder particle size, solid/liquid ratio (S/L = 1, 1.5, and 2) and Al foaming agent content (2–20 wt%) on the expansion and temperature behavior of the slurries were determined in-situ using a laser sensor and a thermocouple, respectively. The geopolymer foams processed using a coarse WG powder slurry, S/L = 2, and 2 wt% Al, were further sintered at 600, 700, 725, and 750 °C. The compression strengths and thermal conductivities of the geopolymer and sintered geopolymer foams were also determined. The slurry expansions continued until about a maximum, and the temperatures of the slurries increased to a maximum, 85–88 °C. At the maximum temperature, the slurry evaporation and the resultant increase in the S/L ratio limited the slurry expansion. Increasing the Al content decreased the final density of the foams (238–555 kg m^{-3}), while the coarse powder slurries resulted in lower densities than the fine powder slurries. Three crystal phases, muscovite, sodium aluminum silicate hydrate, and thermonitrite, were determined in the geopolymer foams. The muscovite formation was noted to be favored at high S/L ratios. During sintering, the partial melting of glass particles started after about 700 °C, while sintering above this temperature decreased the final density of the foams. The reduced density above 700 °C was ascribed to the release of CO_2 due to the decomposition of thermonitrite. Both the compressive strength and thermal conductivity of the geopolymer and sintered geopolymer foams increased with increasing foam density. The highest increase in the compressive strength and reduction in the density were seen in the geopolymer foams sintered at 750 °C.

1. Introduction

Discovered by the French scientist Joseph Davidovits in the 1970s [1], geopolymers are three dimensional amorphous network/chains of tetrahedral silica and alumina linked by covalent bonds similar to the molecular chains in polymers. The details of the geopolymerization reactions are given elsewhere [2]. Briefly, the dissolved species of a precursor material containing silica and alumina in an alkali activation solution form a gel (geopolymer gel), which acts as a cement for the residual precursor. The formed gel is then cured at an elevated temperature in order to obtain a solid form, known as a geopolymer concrete. In addition to the precursor and activation solution, a foaming agent is added to the geopolymer slurries in order to form a cellular-structured product after curing, known as a geopolymer foam. Geopolymer foams are considered an alternative to traditional insulating materials [3] due to their high thermal and fire resistance [4], relatively high compressive strengths, low thermal conductivities, good chemical resistance, and good aging features [5]. So far, geopolymer foams have been mainly investigated using fly ash [2] (FA) and kaolin [6] or met-akaolin (MK) [7] as precursors, sodium hydroxide (NaOH) and sodium silicate (Na_2SiO_3) as alkali activators, and H_2O_2 [3,5,8] and Al powder [3,8-11] as foaming agents. As a foaming agent, H_2O_2 induces uneven large pore sizes [3], while the use of Al powder results in a more controllable pore size distribution [3]. The overall reaction of Al in a NaOH-water solution is [12].

$$2Al(s) + 6H_2O \leftrightarrow 2Al(OH)_3(s) + 3H_2(g) \tag{1}$$
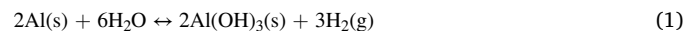
The above reaction starts to release H_2 gas upon dissolution of the thin surface-oxide layer on the Al powder by NaOH. The reaction continues until the H_2 evolution is maximum [13]. Increasing the NaOH/Al molar ratio [14] and decreasing the Al powder particle size increase [12] the H_2 evolution rate. A recent study on a geopolymer slurry of 70 wt% FA and 30 wt% NaOH solution with and without Al addition showed the formation of sodalite ($Na_8(AlSiO_4)6(OH)_24H_2O$) and thermonitrite

($Na_2CO_3 \cdot H_2O$) crystal phases [15]. The kinetics of the geopolymer reactions and the resultant structure are further affected by the ratio of NaOH and Na_2SiO_3 [9]. Utilizing a multi-compound activator of NaOH and Na_2SiO_3 led to a higher slurry viscosity and a higher compressive strength in the obtained geopolymer foam [2].

The re-use of waste streams in manufacturing is of great importance in terms of saving the environment, energy, and natural resources [16,17]. Considering that a very large amount of bottles, windows, and fluorescent and cathode-ray screens are recycled each year (more than 10 million tons in USA alone), the use of waste glass (WG) in geopolymer foam processing looks to be very beneficial not only for saving natural resources but also for eliminating the need for large storage areas for disposal [17,18]. On the other side, the addition of WG powder has already been shown to have a positive effect on the mechanical properties of geopolymer concrete [18]. In addition to this, geopolymer foams were processed using 75 wt% soda-lime WG and 25 wt% MK powder as a precursor and H_2O_2 as a foaming agent. The processed geopolymer foams were then sintered at 700, 800, and 900 °C to obtain glass and glass–ceramic foams [19]. In another study, a waste of tungsten mining powder and WG powder were expanded using a mixture of NaOH and Na_2SiO_3 as an activator and Al powder as a foaming agent [20]. The highest compressive strength was found in the foams cured at 80 °C. The effect of the percentage of Na_2O on the foam density was also shown to be quite substantial in the same study: below 3.1% Na_2O, no foaming occurred due to the absence of NaOH. The final densities of the foams prepared using 3.3 and 3.5% Na_2O solutions varied between 500 and 700 kg m^{-3}.

A short literature review given above has shown a growing recent interest in the use of WG as an additive in geopolymer foam processing. In parallel with this, the present study investigated the possibility of processing geopolymer foams using WG powder as a main precursor. An Al foaming agent powder (Al-11% Si) containing a thick oxide skin layer on the surface was used as an alumina source in addition to the alumina content in the WG powders for the geopolymerization. The effects of WG powder particle size, solid/liquid (S/L) ratio, and Al powder content on the expansion behavior of the geopolymer slurries and the mechanical behavior and thermal conductivities of the obtained geopolymer foams were studied. The geopolymer foams processed using a coarse WG powder slurry (S/L = 2 and 2 wt% Al) were sintered at 600, 700, 725, and 750 °C. Finally, the compressive strengths and thermal conductivities of the prepared geopolymer and sintered geopolymer foams were compared with those published in the literature.

2 Materials and characterization

WG powders were received in two different average particle sizes and used in the expansion/foaming experiments of the geopolymer slurries. The first group of glass powder had an average particle size of 23 μm, which was a residue of a soda-lime window/flat glass polishing facility, Camex (Bursa, Turkey). The second group of WG powder was received from a local supplier in Turkey with an average particle size of 72 μm and obtained by crushing and grinding of the disposed bottles and window glass. The first powder represented a fine particle size, and the second powder represented a coarse particle size. An aluminum powder (90 μm) produced by an open atmosphere melt spinning process was used as a foaming agent in the foaming experiments and also for the alumina source. The activation solution for the foaming experiments of the geopolymer slurries was prepared using Sigma Aldrich NaOH pellets (ACS reagent 97%) and a Na_2SiO_3 solution, also known as water glass (~10.6% Na_2O and ~ 26.5% SiO_2) at a constant Na_2SiO_3/NaOH weight ratio of 2.5. A previous study indicated that a sodium silicate to sodium hydroxide weight ratio of 2.5 resulted in the lowest foam densities using a FA precursor and an Al foaming agent [4]. A Sigma Aldrich carboxymethylcellulose (CMC) (CH_2CO_2H) with an average molecular weight of ~ 90,000 was used as a binder to stabilize and achieve a green strength in the geopolymer foam structure.

A schematic of the slurry preparation and pictures of the foam expansion and temperature measurement set-up are shown in Fig. 1. The foamable geopolymer slurry preparation started by dissolving CMC (3 wt% of a 112 gr of foamable slurry) in distilled water at room temperature on a magnetic stirrer. NaOH pellets with an amount that would give an 8 M solution were then added to the CMC solution while the solution was continuously mixed. The Na_2SiO_3 solution was then added at an amount that would give an S/L ratio of 1, 1.5, and 2, and the solution was mixed in a high-speed mechanical mixer for 1 min. Sequentially, appropriate amounts of WG and Al powder were then added, and the resultant slurry was mixed in a high-speed mechanical mixer for 5 and 2 min, respectively. The prepared geopolymer slurry was then poured into a transparent Plexiglas foaming tube having a diameter of 73 mm, a height of 150 mm, and enclosed at the bottom. The expansion and the temperature of the slurries were measured in-situ inside the foaming tube. The used coding, the S/L ratios, and the amount of the constituents of the investigated geopolymer slurries are tabulated in Table 1. The solid to liquid ratio was calculated in gram-ratio. The liquid weight was calculated by adding the weights of the water, Na_2SiO_3 solution, and solids (NaOH pellets and CMC powder) dissolved in the liquid. The solid weight was calculated by adding the weights of the WG and Al powder. The wt% of Al was calculated by dividing the weight of the Al powder by the total weight of the solid (Al + WG) and multiplying the result by 100. As tabulated in Table 1, the effect of the Al content (2–20 wt%) on the expansion was investigated using the fine powder slurries (1, 1.5, and 2), and the effect of the S/L ratio was investigated using the coarse powder slurries. A laser sensor (Micro Epsilon ILR1030-8) clamped by a holder at a distance of 20 cm above the foaming tube, as shown in Fig. 1, was used to measure the expansions of the slurries in-situ. The sensor was operated between 4 and 20 mA and calibrated before each experiment by determining the corresponding current difference of a known distance. The temperatures of the foaming slurries were measured by using a K-type thermocouple that was dipped into the slurry near the bottom of the Plexiglas foaming tube. The simultaneous changes in the expansions and temperatures of the slurries were then recorded by a Data Taker DT 80 data logger, and then the data were transferred to a computer. The percent of volume expansion (V_E (%)) or linear expansion was calculated using the following relation

$$V_E(\%) = \frac{h_f - h_i}{h_i} x100 \qquad (2)$$

where h_f and h_i are the final and initial height of the slurry, respectively. The foamed slurries were kept at room temperature for 24 h inside the foaming tube. The foams were then removed from the foaming tube (see a removed foam cylinder in Fig. 2) and then cured in an oven at 60 °C for 24 h. The cured foams prepared by using the coarse powder slurry, S/L = 2 and 2 wt% Al, and coded M0 in Table 1 were sintered at 600, 700, 725, and 750 °C for 1 h in a Protherm Laboratory Furnace (Model PLF 130/5). These foams were heated at a heating rate of 10 °C min^{-1} to the sintering temperature, kept at the sintering temperature for 1 h, and then furnace-cooled to room temperature.

The compression tests on the geopolymer and sintered geopolymer foams were conducted on the cylindrical test samples, 20 ± 0.05 mm in diameter and 25 ± 1.2 mm in length, in a SHIMADZU AG-I universal testing machine at a strain rate of 1×10^{-3} s^{-1} at room temperature. The compression test samples shown in Fig. 2 were extracted from the cured and sintered foam cylinders (7.3 mm in diameter) by using a core-drilling machine. Core-drilling was made without a liquid coolant. Three compression test samples were extracted from each foam cylinder (Fig. 2). The top and bottom surfaces of the core-drilled compression cylindrical test samples were then made parallel by dry grinding. The grinding was made inside a parallel-surfaced rectangular steel block having a central cylindrical hole that had a diameter slightly larger than that of the foam compression test sample. The sample was inserted inside the hole, and the foam test sample and the steel block were dry-
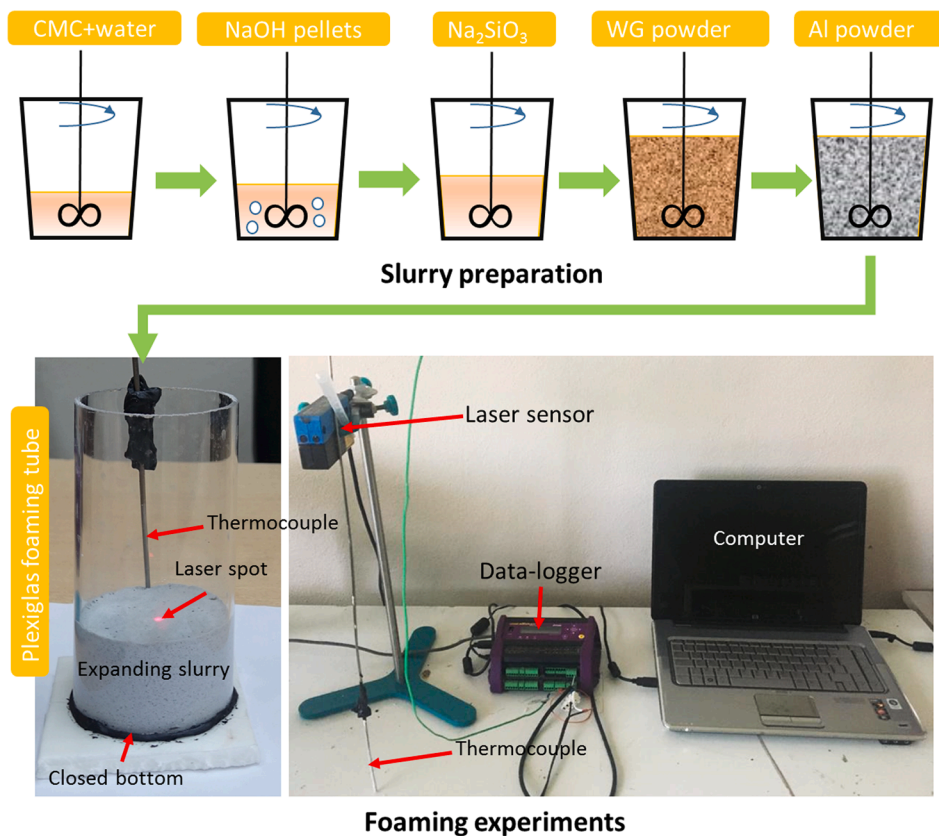
Fig. 1. The schematic of the slurry preparation and foam expansion and temperature measurement set-up.

Table 1
The coding, S/L ratios, and amount of the constituents of the investigated geopolymer slurries.

No	S/L	Water(mL)	Al (wt%)	Al(gr)	NaOH (gr)	CMC(gr)	Na$_2$SiO$_3$(mL)	Glass powder (μm)
S0	1	18.5	2	1.1197	5.92	1.68	21.5	23
S1	1	18.5	4	2.2394	5.92	1.68	21.5	23
S2	1	18.5	8	4.4788	5.92	1.68	21.5	23
S3	1	18.5	12	6.7182	5.92	1.68	21.5	23
S4	1	18.5	16	8.9576	5.92	1.68	21.5	23
S5	1	18.5	20	11.197	5.92	1.68	21.5	23
L0	1	18.5	2	1.1197	5.92	1.68	21.5	72
L1	1	18.5	4	2.2394	5.92	1.68	21.5	72
L2	1	18.5	8	4.4788	5.92	1.68	21.5	72
N0	1.5	14.8	2	1.3436	4.736	1.34	17.2	72
N1	1.5	14.8	4	2.6872	4.736	1.34	17.2	72
N2	1.5	14.8	8	5.3745	4.736	1.34	17.2	72
M0	2	12.33	2	1.4929	3.946	1.12	14.33	72
M1	2	12.33	4	2.9858	3.946	1.12	14.33	72
M2	2	12.33	8	5.9716	3.946	1.12	14.33	72

A total of 112 g of slurry was prepared.

ground together. By this way, the surfaces of the test samples were made parallel to each other. Dust accumulated on the surfaces of the samples during core-drilling and grinding was removed by applying compressed air. The density of the compression test samples was measured by dividing the weight by the total volume. The foam expansion direction was the compression axis of the test samples, as shown by an arrow in Fig. 2. A video extensometer was used to measure the displacements during the tests, and the deformation of the samples during the tests was recorded by a video camera. At least three tests were performed for each group of foam samples. The nominal strain was calculated by dividing the machine stroke by the length of the long axis of the test sample, and the stress was calculated by dividing the force by the cross-sectional area.

The thermal conductivities of the obtained foam samples were measured in a KEM QTM 500 thermal conductivity meter. The foam samples for thermal conductivity measurements were 120 mm × 60 mm × 20 mm in size and prepared separately inside a rectangular plastic mold. After curing and/or sintering, the top and bottom surfaces of these samples were ground until the surfaces were parallel and flat. The thermal conductivity was measured along the foaming direction. At least three thermal conductivity measurements were taken for each group of foam samples, and the results were averaged.

The elemental composition of the raw materials was determined in a Spectra IQ II X-ray fluorescence spectrometer. The X-ray diffraction (XRD) analysis of the prepared foams was performed in a Philips X'Pert Pro X-ray diffractometer using CuKα radiation (1.5418 Å) at 40 kV from 5 to 80° with a 0.05° s^{-1} scanning rate. The fracture surfaces of the tested samples were examined by an FEI QUANTA 250 FEG scanning electron
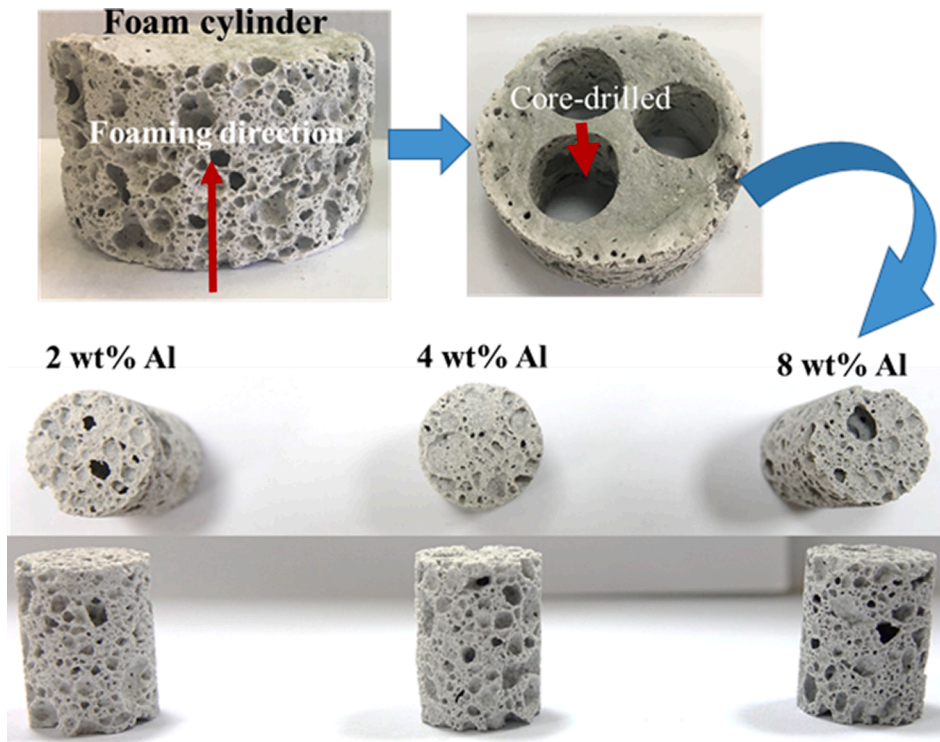
Fig. 2. The pictures of a foam and a core-drilled foam cylinder (prepared using coarse powder slurries with an S/L ratio of 2 and different aluminum content) and the foam compression test samples after core-drilling.

microscope (SEM), and the microstructural analysis was performed in the backscattered electron mode using an Everhart-Thornley detector and energy dispersive X-ray analyzer. The samples for the microstructural analysis were mounted in epoxy and sequentially ground and polished down to 1 μm. The molecular bond and the structure of the foams were determined by using a Digilab Excalibur Series Fourier transform infrared spectroscopy (FTIR) device with the attenuated total reflectance method.

3 Results and discussion
3.1 Powder characterization

The XRF analyses of the fine and coarse size glass powders are tabulated in Table 2. The used WG powders have similar compositions, except the coarse powder contains a slightly higher Al_2O_3 content (1.6%) than the fine powder (1.4%). The average particle sizes of the fine and coarse powders were previously determined and were ~ 23 μm [21] and 72 μm [22], respectively. Ninety percent of the fine powder particles were less than 60 μm, and 10% were less than 4 μm. The coarse powder had 90% of its particles less than 340 μm, and 10% of the particles were less than 11 μm. The glass particles had angular shapes in small and large sizes. The XRD of both glass powders indicated an amorphous structure. The used foaming agent was essentially an Al-Si alloy powder containing 11% Si as a major element. The aluminum powder particles were irregular in shape and slightly elongated through one axis with an average particle size of 90 μm, which was also confirmed by the optical microscope measurements. The powder contained about 5% oxide skin layer, as reported by the producer.

Table 2
The compositions of WG powders used.

Waste glass	SiO_2	Al_2O_3	Na_2O	CaO	MgO
Fine powder weight (%)	73	1.4	12	12	1.6
Coarse powder weight (%)	73	1.6	12	11.5	1.75

3.2 Slurry expansions

The representative expansion-time and temperature–time curves of the studied geopolymer slurries are shown in Fig. 3. Similar expansion-time and temperature–time curves of two foaming experiments of the same slurry (fine powder, S/L = 1 and 8 wt% Al) shown in Fig. 3 confirm the repeatability of the foaming experiments. Furthermore, three characteristics of the foam expansion curves are marked by the circled
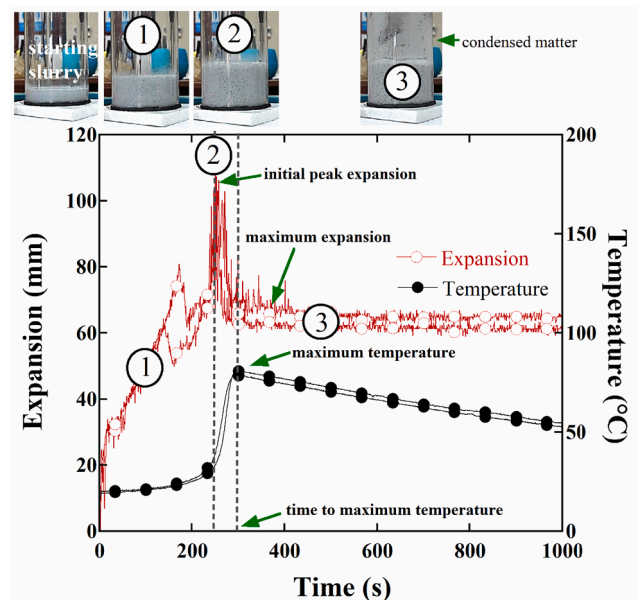

Fig. 3. The representative expansion-time and temperature–time curves and the pictures of the expanding slurry in the foaming tube at various times (two foaming experiments, fine powder, S/L = 1, and 8 wt% Al).

numbers in the same figure. These are (1) a rapid expansion region at the initial stage of foaming, which is followed by (2) an initial peak expansion and (3) a nearly constant expansion region after the initial peak expansion. The pictures of the foaming tube of an expanding slurry in region 1 at the initial peak expansion (2) and in region 3 are also shown at the top of Fig. 3. The starting height of the slurry is about 20 mm. Then, it rapidly increases above 100 mm in region 1 until about the initial peak expansion (2). The expansion, thereafter, sharply decreases to 60–65 mm. The matter in the escaped gas condenses on the interior surface wall of the foam expansion tube, as seen in Fig. 3. In the present study, the expansion in region 3 of Fig. 3 is considered as the maximum expansion. A gradual increase in the temperature of the slurry at the beginning of foaming is seen in region 1 (the first dotted line in Fig. 3). This is followed by a rapid-rise to a maximum value until about the initial peak expansion (the second dotted line in Fig. 3); thereafter, the temperature decreases gradually to room temperature. The maximum temperature in the temperature–time curve is further considered as the maximum temperature, and the corresponding time is taken as the time to reach maximum temperature (Fig. 3). The representative expansion-time and temperature–time curves of the fine and coarse glass powder slurries with S/L = 1 at increasing wt% Al are shown in Fig. 4(a) and (b), respectively. These expansion-time and temperature–time curves also exhibit the characteristics outlined above. The maximum percent

volume expansion and temperature of all fine and coarse powder slurries studied are further tabulated in Table 3 together with the density and compressive strengths of the resultant geopolymer and sintered geopolymer foams. In general, the volume expansions of the fine and coarse powder slurries show very similar trends, and both tend to increase with increasing Al content (Table 3) except the slurries with high Al and solid content (fine powder slurry with 20 wt% Al and coarse powder slurry with S/L = 2). The expansion of the slurries occurs via H_2-bubble formation, concurrently proceeding by a nucleation and diffusion stage. High pressure developed in the initial nucleation stage results in a sudden expansion of the slurries [23,24]. The observed initial peak expansions in the expansion-time curves of the slurries in Fig. 4(a) and (b) are most likely due to this effect. The following two reactions give rise to H_2 evolution [12],

$$2Al + 6H_2O + 2NaOH \rightarrow 2NaAl(OH)_4 + 3H_2 \tag{3}$$

$$NaAl(OH)_4 \rightarrow Al(OH)_3 + NaOH \tag{4}$$
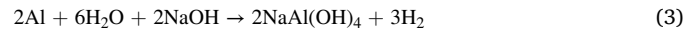
The H_2 generation in the above reactions is controlled by the NaOH/Al weight ratio. If the ratio is lower than the stoichiometric one, ~1.48, a lower amount of H_2 is generated [12]. Reaction (4) is triggered when the amount of $NaAl(OH)_4$ reaches a super-saturation point; therefore, reaction (3) is not triggered at very low NaOH/Al ratios.

For the studied slurries having 5.92, 4.736, and 3.946 g of NaOH (Table 1), the stoichiometric weights of Al are 4, 3.2, and 2.66 g, respectively. When the NaOH/Al weight ratio is higher than the stoichiometric ratio of 1.48 (underlined in Table 3), the added-Al powder is presumed to completely react with water; hence, it limits both the volume expansion and the temperature of the slurries. These slurries, as tabulated in Table 3, exhibit both relatively low volume expansions and low temperatures due to the lesser amount of Al added.

Since the hydrogen generation reaction is exothermic (reaction (3)), the temperature of the slurry increases as the expansion proceeds [13]. The rise in temperature increases both the S/L ratio of the slurries (due to rapid evaporation of the liquid) and the geopolymerization reaction rate. Both increase the apparent viscosities of the slurries, leading to the termination of the expansions (solidification) in the slurries with a NaOH/Al weight ratio lower than 1.48 (excess amount of unreacted Al powder). The termination of the expansions occurs at the maximum temperature (saturation temperature), which nearly corresponds to 12 wt% Al in the fine powder slurries and 4–8 wt% Al in the coarse powder slurries (Table 3). On the other side, an increase in the solid fraction also increases the apparent viscosity of the slurries [25]. The increase in the expansions of the coarse powder slurries with S/L = 1.5 and 2 at and above 4 wt% Al and the fine powder slurries at and above 8 wt% Al in Table 3 (having the same maximum temperature) may be partly due to the increased apparent viscosities of the slurries with the presence of an excess Al powder over the stoichiometric amount. For example, the excess amount of Al increases from 0.326 g at 4 wt% Al to 3.3 g at 8 wt% Al for the coarse powder slurries at the S/L = 2. Although the volume expansion of the coarse powder slurries with the addition of 2 wt% Al increases from 109 to 278% when the S/L increases from 1 to 1.5, the maximum volume expansion of the S/L = 2 slurries is 235%, below that of the S/L = 1.5 slurries. At the S/L ratio of 2, the coarse powder slurry is thicker, and there is also a lesser amount of NaOH than the slurry with S/L = 1.5 (Table 1). The excessive increase in the viscosity and the lesser amount of Al reacted in the coarse powder slurries with the S/L of 2 may result in lower expansion in these slurries than the slurries with the S/L ratio of 1.5. The excessive increase in the viscosity may also apply to the expansion of the fine powder slurries with 20 wt% Al added.

As tabulated in Table 3, the maximum temperatures of the fine and coarse powder slurries with the S/L = 1 saturate at about 85 °C. The maximum temperatures of the coarse powder slurries with the S/L = 1.5 and 2 are very similar to each other, and both saturate nearly at the same maximum temperature, ~88 °C. The temperature rise for a constant amount of NaOH solution was previously reported to increase with
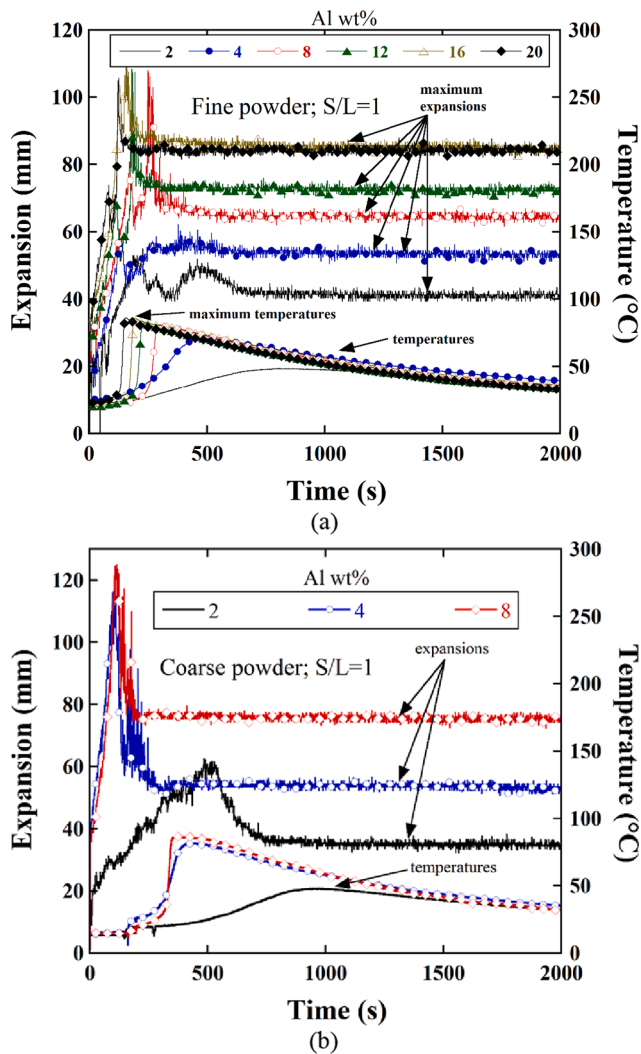

Fig. 4. The representative expansion-time and temperature–time curves of (a) fine powder and (b) coarse powder slurries with S/L = 1 and increasing wt% of Al.

Table 3
The maximum volume expansion and temperature of the slurries and the density and compressive strength of the geopolymer and sintered geopolymer foams.

No	S/L	Al (wt%)	NaOH/ Al(gr-ratio)	Maximum volume expansion (%)	Maximum temperature (°C)	Density (kg m^{-3})	Compressive strength (MPa)
S0	1	2	5.287	158 ± 5.6	49.7 ± 4.7	555 ± 47	3.00 ± 0.095
S1	1	4	2.643	235 ± 1.88	69 ± 1.68	372 ± 22	1.20 ± 0.22
S2	1	8	1.321	300 ± 15.7	81 ± 3.10	342 ± 6.6	1.05 ± 0.13
S3	1	12	0.881	359 ± 27.6	84 ± 1.30	306 ± 27.5	1.02 ± 0.05
S4	1	16	0.660	423 ± 31	85 ± 0.72	279 ± 2.33	0.62 ± 0.47
S5	1	20	0.528	389 ± 29	85 ± 0.55	280 ± 55	0.53 ± 0.03
L0	1	2	5.287	109 ± 2.3	47.9 ± 0.7	520 ± 22	1.84 ± 0.57
L1	1	4	2.643	229 ± 13.8	80.5 ± 1.68	296 ± 10	0.18 ± 0.04
L2	1	8	1.321	337 ± 8.2	86 ± 1.70	238 ± 8.2	0.21 ± 0.07
N0	1.5	2	3.526	278 ± 7.46	70.5 ± 1.35	400 ± 11.6	0.707 ± 0.12
N1	1.5	4	1.762	354 ± 11.9	88.4 ± 0.67	318 ± 18.2	0.54 ± 0.16
N2	1.5	8	0.881	430 ± 12.5	88.7 ± 1.1	295 ± 27	0.29 ± 0.09
M0	2	2	2.643	235 ± 19.9	80 ± 1.40	457 ± 9.80	0.94 ± 0.19
M1	2	4	1.321	301 ± 8.9	89 ± 1.30	421 ± 13.2	0.90 ± 0.16
M2	2	8	0.660	379 ± 12	88.5 ± 1.94	349 ± 2.30	0.72 ± 0.17
M0-600 °C	2	2	–	–	–	450 ± 26	0.81 ± 0.15
M0-700 °C	2	2	–	–	–	440 ± 22	1.10 ± 0.14
M0-725 °C	2	2	–	–	–	390 ± 32	1.45 ± 0.05
M0-750 °C	2	2	–	–	–	380 ± 12	2.20 ± 0.15

increasing Al addition until about a saturation temperature between 95 and 100 °C (the boiling point of water) [26]. The lower saturation temperatures of the present study, 85–88 °C, may be partly due to the presence of WG particles and partly due to the fact that the temperature of the slurries was measured at the bottom of the foaming cylinder. The temperature at the top is expected to be higher than at the bottom since the generated H$_2$ gas moves upward.

The densities of the obtained foams vary with the Al wt%, as tabulated in Table 3. In general, increasing the Al content decreases the final foam densities as the expansion increases. Increasing the S/L ratio increases the densities of the foams of the coarse powder slurries except for the foams of the slurries with the S/L = 1 at 2 wt% Al. The densities of the foams of this slurry is higher than those of the slurries with the S/L = 1.5 and 2. This is due to the large drops in the expansions (collapse of cellular structure due to low viscosity) after the initial peak expansion (Fig. 3), leading to high final foam densities. These results, furthermore, confirm that both the Al content and the S/L ratio of the slurries are effective in altering the final densities of the resultant geopolymer foams.

As the slurry expansion is terminated at the maximum temperature, the corresponding time is taken as the time to maximum expansion. Fig. 5 shows the variation of the time to maximum temperature of the fine and coarse powder slurries with Al content at different S/L ratios. At 2 wt% Al, the fine powder slurry shows a lower time to maximum (A in

Fig. 5) than the coarse powder slurry (B in Fig. 5). The expansion rate is, therefore, faster in the fine powder slurries at low Al wt%, but at increasing Al wt%, the time to maximum of the fine and coarse powder slurries becomes almost similar to each other. Also, increasing the S/L ratios of the coarse powder slurries at 2 wt% Al decreases the time to maximum due to the higher particle content of the higher S/L ratio slurries, leading to a quick slurry thickening. The time to maximum, however, should be approached carefully. Since the hydrogen evolution is very rapid in the slurries with a high amount of Al added, even in the mixing stage, the foaming might start. Nonetheless, Fig. 5 shows a general trend of the expansion limit time of the studied geopolymer foams.

The previous studies showed that the foam density increased as the sintering temperature increased due to the shrinkage resulting from glass particle fusion [27]. The present study showed a reverse effect. As will be elaborated in section 3.5, the reduced density of the present sintered foams is mainly due to the decomposition of thermonitrite at elevated temperatures, giving rise to CO$_2$ evolution and, hence, resulting in an expansion of the softened foam over the contraction due to the sintering shrinkage. The coarse powder geopolymer foams processed with S/L = 2 and 2 wt% Al has a mean density of 457 kg m^{-3}, and sintering at 600 °C results in a relatively small change in the foam density (Table 3). However, the mean densities of the foams sintered at 700, 725, and 750 °C decrease to 440, 390, and 380 kg m^{-3}, respectively. Although the diameter and height of the geopolymer foam stay almost the same as the unsintered one when sintered at 600 °C, the diameter of the foams increases (Fig. 6(a-c)) and the height decreases (Fig. 6(b)) after sintering above 700 °C. Also, when the sintering temperature is above 700° C, the glass particles are semi-melted and diffuse into each other, an effect particularly seen at 750 °C in Fig. 7(d).

3.3 Compressive strength and thermal conductivity of geopolymer and sintered geopolymer foams

The compression stress–strain curves (2 tests for each density) of the geopolymer foams of three different densities processed using the fine powder slurries are shown in Fig. 7(a). A picture of a geopolymer foam compression test sample is also shown in the inset of Fig. 7(a). The sample fails in a brittle manner following a maximum stress or compressive strength by forming axial cracks along the loading axis (Fig. 7(a)). All compression test foam samples exhibited the same brittle type of fracture behavior. Furthermore, the compressive strength increases as the density of the foams increases regardless of the S/L ratio and wt% Al. For example, the compressive strength of the foams of the fine powder slurries increases from ~ 0.5 to ~ 3 MPa when the density
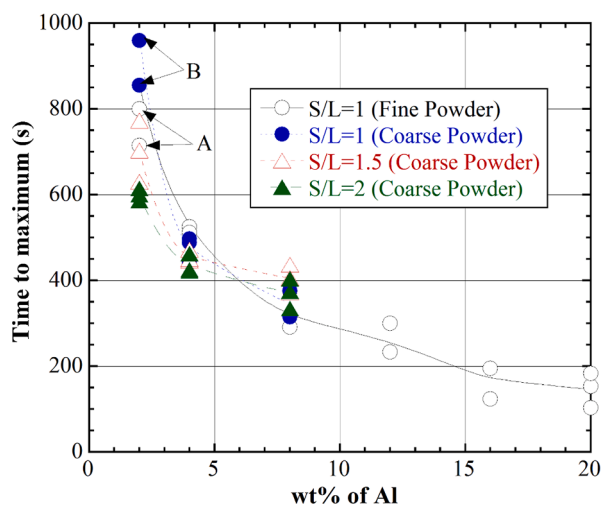
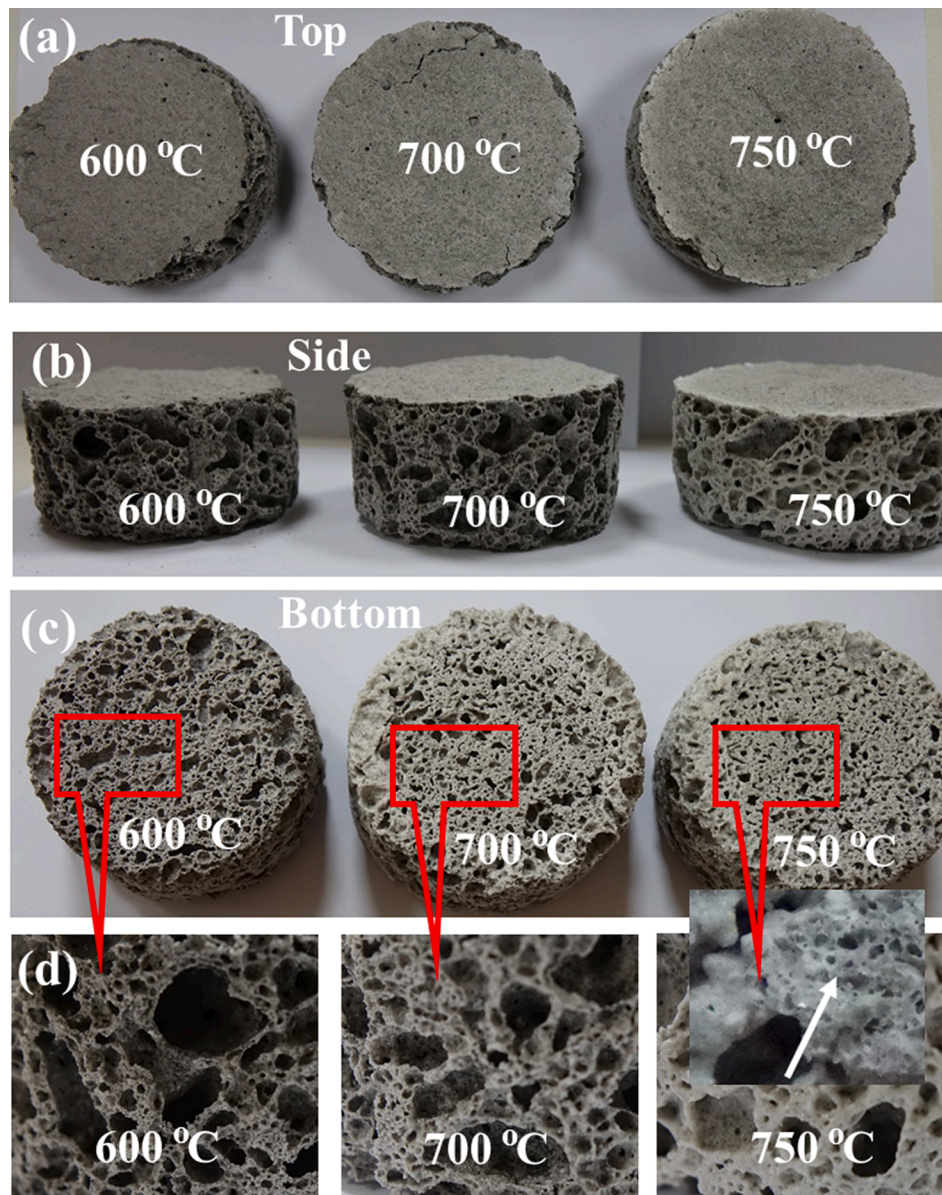**Fig. 5.** Time to maximum temperature vs. wt% of Al.

Fig. 6. The images of sintered foams (a) top, (b) side, and (c) bottom views, and (d) magnified images showing the cell structure at different temperatures.

increases from 280 to 555 kg m^{-3} (Fig. 7(a)). The representative compressive stress–strain curves of the geopolymer foams (coarse powder, S/L = 2, and 2 wt% Al) sintered at 600, 700, 725, and 750 °C are shown in Fig. 7(b) together with that of the unsintered foams. Note that the compressive strength of the foam sintered at 600 °C is very similar to that of the unsintered foam at the same density. The effect of the sintering temperature on the compressive strength starts to be seen at and after about 700 °C (Fig. 7(b)). As tabulated in Table 3, the greatest increase in the compressive strength is seen in the foams sintered at 750 °C. The compressive strength of the foams sintered at this temperature is almost two times that of the unsintered foam sample. Regardless of the foam density, the geopolymer and sintered geopolymer foams also failed by axial cracks starting from either the upper or bottom of the compression test platens. After the formation of the cracks, the deformed foam sample stayed in contact with the compression test platens, and the unfractured pieces continuously compressed and fractured, leading to a plateau stress region after the compressive strength in the stress–strain curves. The compressive fracture strength of brittle foams (σ_f) was proposed to follow the following equation [28].

$$\sigma_f = \sigma_s[C(\varphi\rho_{rel})^{\frac{3}{2}} + (1 - \varphi)\rho_{rel}] \tag{5}$$

where σ_s is the strength of the cell wall material (the fracture strength of glass was reported to be 70 MPa [29]), C is a constant (given as 0.2 in [28]), ρ_{rel} is the relative density of the foam ($\frac{\bar{\rho}}{\rho_s}$, where $\bar{\rho}$ is the density of the foam and ρ_s is the density of the solid), and φ is the volume fraction of the solids contained on the plateau borders. The first term in Eqn. (5) is due to cell edge bending, and the second term is due to the cell wall membrane stretching. The compressive strengths of the prepared geopolymer and sintered foams and the previously investigated geopolymer foams processed using Al [3,4,30] and glass foams [21,31-45] are shown as a function of foam density in Fig. 7(c). Although the foams of the fine powder slurries exhibit higher compressive strengths than those of the coarse powder slurries at low geopolymer foam densities (~300 kg m^{-3}), both powder foams show similar compressive strengths at about 500 kg m^{-3}. The compressive strength of the prepared geopolymer foams is also comparable with those of the previous studies on different precursors. The compressive strengths of the present and previous geopolymer foams in Fig. 7(c) range 0.2–4 MPa and approach the
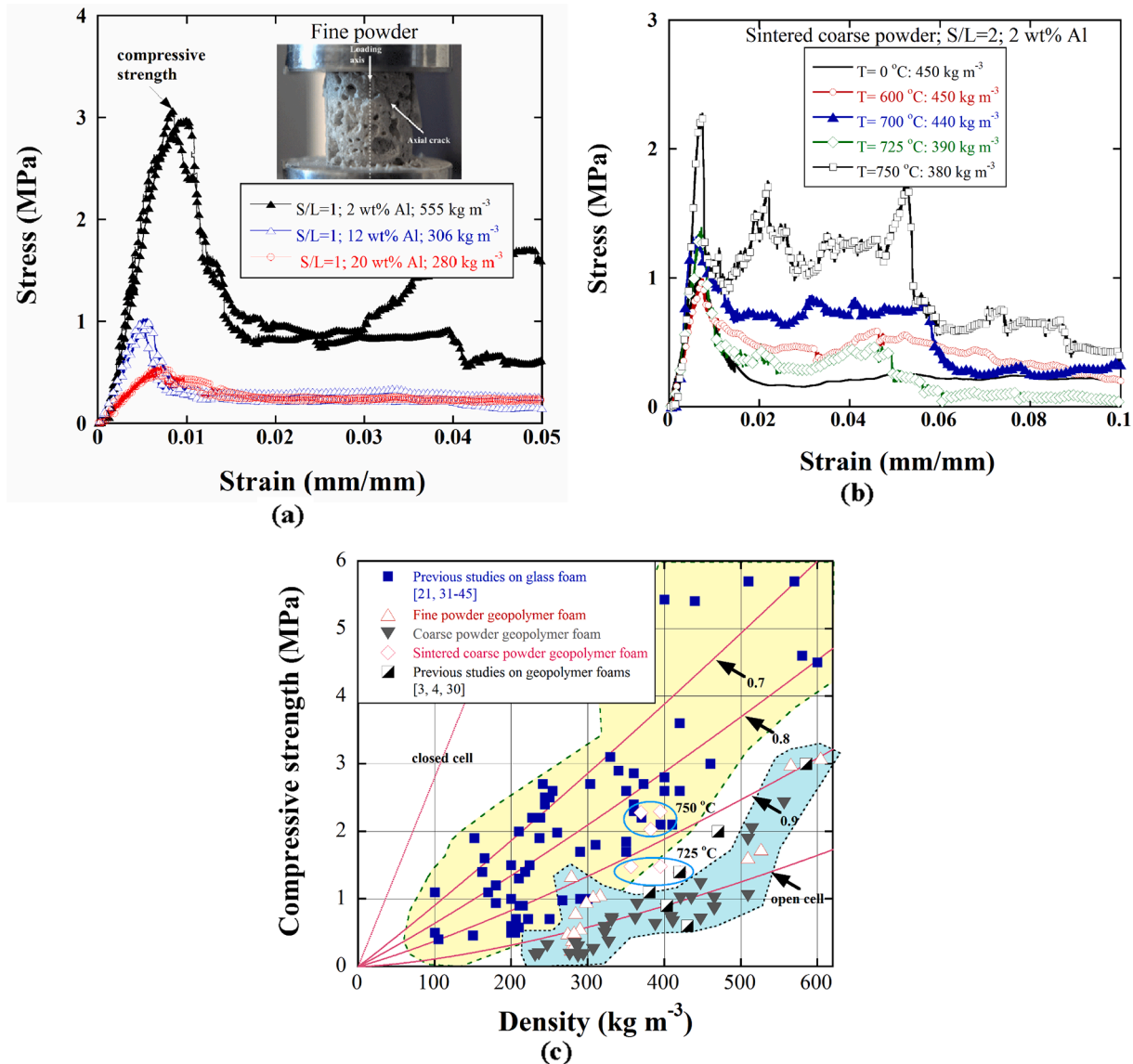
Fig. 7. (a) The compressive stress–strain curves of the geopolymer foams processed using fine powder, (b) the representative compressive stress–strain curves of geopolymer foams sintered at different temperatures, and (c) the variations in the compressive strengths of the present geopolymer and sintered geopolymer foams and the previously investigated geopolymer and glass foams with density.

compressive strengths of the open-cell glass foams predicted using Eqn. (5) (lower line in Fig. 7(c)). The compressive strengths of the reported glass foams are further well fitted with φ values between 0.7 and 0.9 for the foam densities between 300 and 600 kg m^{-3} (Fig. 7(c)). The compressive strengths of the geopolymer foams sintered at 750 °C fall at the lower range of the compressive strengths of previous studies at about 400 kg m^{-3}. However, the tested present geopolymer foam samples show a lower compressive strength than those of previously studied glass foams. One of the reasons for that is that the cell edges and walls in the present geopolymer foams contain pores in between the glass powder particles. The pores in the cell edges and walls tend to weaken the compressive strength by forming high-stress concentration sites.

The average thermal conductivities of the foam samples at three different densities (585, 535, and 462 kg m^{-3}) processed using the coarse powder slurries at 2 wt% Al but at different S/L ratios (1, 1.5, and 2) are tabulated in Table 4 together with the average thermal conductivity of the foam sintered at 750 °C (368 kg m^{-3}). As the samples for the thermal conductivity measurement were processed in a rectangular shape, their densities were also higher than those of the cylindrical samples. The thermal conductivities are also a function of density and

Table 4

The thermal conductivities and the corresponding densities of the foam and sintered foam samples processed using the slurries with 2 wt% Al (foam samples for the thermal measurement were prepared separately).

Sample name	S/L ratio	Density (kg m^{-3})	Average thermal conductivity (W m^{-1} K^{-1})
L0	1	585	0.1808 (0.1617–0.1985)
N0	1.5	535	0.1158 (0.1042–0.1230)
M0	2	462	0.1100 (0.0888–0.1289)
M0-750 °C	2	368	0.0780 (0.0672–0.0934)

increase as the foam density increases. The lowest average thermal conductivity is found in the sintered foam at 368 kg m^{-3}, 0.078 W m^{-1} K^{-1}, and the highest thermal conductivity in the highest density foam, 0.1808 W m^{-1} K^{-1} at 585 kg m^{-3}. The variations in the thermal conductivities of the prepared geopolymer and sintered geopolymer foams at 750 °C with density are shown in Fig. 8 together with those of previously investigated geopolymer [3,4,8-11,16,30,46-49] and glass foams [31,37,43,50-52]. The thermal conductivities of the prepared
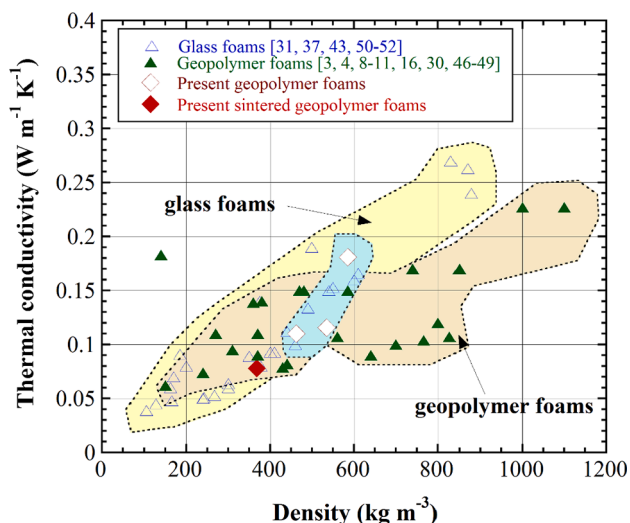
Fig. 8. The variations in the thermal conductivities of the present geopolymer and sintered foams and the previously investigated geopolymer and glass foams with density.

geopolymer and sintered geopolymer foams are comparable with the reported values of the thermal conductivities of similar foams. However, glass foams exhibit higher thermal conductivities than geopolymer foams at high densities. It is also seen that the starting silica raw material has an effect on the thermal conductivities. The foams processed with the slurries containing WG basically show lower thermal conductivities at the same foam densities, as seen in Fig. 8.

3.4 Microstructural and microscopic analysis

Depending on the network between Si-Al, geopolymer foams were reported to have either an amorphous or semi-crystalline structure [27]. The prepared geopolymer and sintered geopolymer foam samples showed low crystallinities similar to a previous study [9]. The main crystal phases detected include thermonitrite ($Na_2CO_3 \cdot H_2O$) (Ref. No: 00–008–0448), sodium aluminum silicate hydrate (SASH) (Na_2Al_2-$Si_{17.5}O_{35.4} \cdot 8H_2O$) (Ref. No: 00–035–0375), and muscovite (NaAl$_2$(AlSi$_3$O$_{10}$)(OH)$_2$) (Ref. No. 00–046–1311). SASH was only found in the geopolymer foam samples prepared using the slurries with S/L = 1, while thermonitrite and muscovite were found in all geopolymer foam samples. The XRD patterns of the sintered foams, however, exhibit only muscovite and SASH phases, as seen in Fig. 9(a). The formation of muscovite and SASH crystalline phases depends on the amount of oxygen in the foams [1]. The sintering in an open atmosphere increases the oxygen content of the foams and, hence, promotes the formation of SASH and muscovite. The observed thermonitrite formation in the geopolymer foams was attributed to the atmospheric carbonation of NaOH and the increase in free alkali in the geopolymer matrix [15,27,53]. The thermonitrite decomposes at elevated temperatures and gives rise to CO_2 gas based on the following reaction

$$Na_2CO_3 \rightarrow Na_2O + CO_2(g) \tag{6}$$

The use of a carbonate-based binder (CMC) in the present study further intensified the formation of thermonitrite. Sintering at high temperatures decomposes thermonitrite, releasing CO_2 gas and leading to the formation of small gas bubbles on the cell walls and edges when the glass particles were in a semi-melt state (shown by an arrow in the foams sintered at 750 °C in Fig. 6(d)). The sintering process provides compactness to the sintered foams by bonding glass particles and reduces the density of the foam by forming small pores on the cell walls and edges. Both result in the development of high strength and low density in the sintered foams, particularly in the foams sintered at

750 °C. The FTIR analysis of the coarse powder geopolymer foams processed with different Al content at the S/L = 2 are shown in Fig. 9(b) together with that of the WG powder. The bond at 771 cm^{-1} is only seen in the FTIR analysis of WG and refers to the Si-O bond in the SiO$_4$ tetrahedron. The main bond around 975 cm^{-1} is due to the stretching vibration of the Si-O-Si bond. Normally, the Si-O-Si vibration occurs at around 980–1000 cm^{-1}, while the presence of the Si-O-Al bond shifts this wavenumber slightly to lower values (Fig. 9(b)). The shift is also seen in the FTIR analysis of WG due to the alumina content of the glass powder (1.6%). The peak at about 1435 cm^{-1} is due to the O-C-O stretching and only seen in geopolymer foams. The FTIR analysis of the sintered foams prepared using coarse powder slurries, S/L = 2, and 2 wt % Al at different temperatures are shown in Fig. 9(c). The main bonds around 946 cm^{-1} are due to the stretching vibration of the Si-O-Si bond. As noted in the same figure, the carbonate vibration at 1435 cm^{-1} disappears after sintering, proving the decomposition of thermonitrite. The characteristic bonds of the WG powder located at 975 and 771 cm^{-1} in Fig. 9(b) also disappear after the formation of a gel network. The bonds that exist in these two wavenumbers are decomposed by the reactions in the alkaline medium as [54]

$$\equiv Si - O - Si \equiv + OH^- \rightarrow \equiv Si - OH + \equiv Si - O^- \tag{7}$$
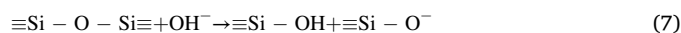
Thereafter, the Si-O-Al bond formation with Al occurs at around 1000 cm^{-1} [27]. Due to the formation of an aluminosilicate gel, the Si-O-Al bond formation shifts to around 975 cm^{-1} for all S/L ratios and Al content [3]. The intensity of the bond is related to the participation of water in a reaction of non-bridging oxygen enhancement [15]. As the alkaline amount increases, the main bond shifts towards smaller wavenumbers. This is due to the increase in the number of silicon sides with non-bridging oxygen balanced by sodium cations. In addition, the increase in alumina in the structure reduces the wavenumber because of the enhancement of the silicate network containing the tetrahedral Al [9]. The highest shift seen in the geopolymer foams processed using 2 wt % Al (Fig. 9(c)) is explained by the shift of the wavenumber back to a higher wavenumber with the increase in Si participating in the geopolymerization reaction [15]. The increase in Si in the reaction is higher as the amount of reacted Al increases. The wavenumber shifts up to 946 cm^{-1} in the sintered geopolymer foams (Fig. 9(c)).

The SEM micrographs of the polished cross-sections of the geopolymer foam processed using coarse powder slurry, S/L = 2, and 2 wt% Al are shown at a low and high magnification in Fig. 10(a) and (b), respectively. The black regions seen in the same micrographs are the epoxy mounting material. A cellular structure with varying cell sizes is apparent in Fig. 10(a). The packing of smaller size glass particles in between larger particles on the cell walls is seen in Fig. 10(b). The particle packing on the cell walls was observed to increase with increasing S/L ratio. Extensive glass particle cracking at the interface of the geopolymer gel are also detected, as marked by an ellipse in Fig. 10 (b). The cracking may be due to the differences in the thermal expansion coefficients between the geopolymer gel and the glass particles and likely occurred during the foam preparation and curing stage. Fig. 10(c) shows the elemental line scan of the glass particles and the geopolymer gels in between the glass particles. As seen in the figure, the geopolymer gels contains a lower Na and Si content but a higher Al content than the glass particles.

The SEM micrograph of a fractured geopolymer foam sample processed using the coarse powder slurries, S/L = 1.5, and 2 wt% Al is shown in Fig. 11(a). A close inspection of the cell walls in the same figure reveals the 3D-bonded networks of the glass particles. The precipitates of Na-Al-Si also form a nearly continuous phase on the surfaces of the glass particles, as shown in the inset of Fig. 11(a). The particle bonding by the geopolymer gel was further observed to intensify when the S/L ratio increased. The SEM images of the fracture surfaces of the foam samples sintered at 700, 725, and 750 °C are shown in Fig. 11(b-c) at the same magnification, respectively. Sintering at 600 °C had no effect on
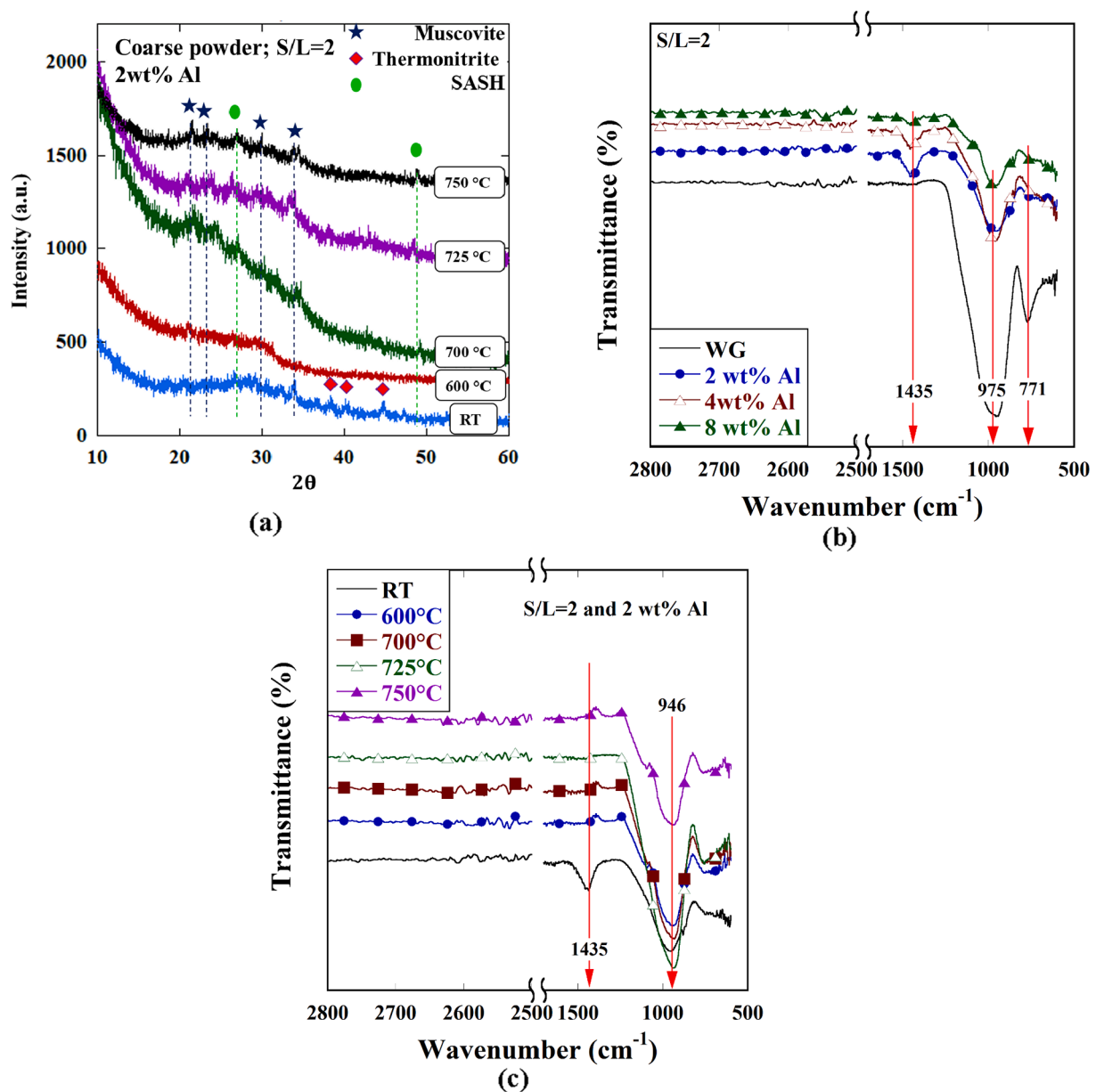
Fig. 9. (a) The XRD pattern of geopolymer and sintered geopolymer foams processed using the coarse powder slurries and S/L = 1 and the FTIR analysis of (b) the geopolymer and (c) sintered geopolymer foams processed using the coarse powder slurries and S/L = 2.

the cell structure of the foams, while the glass particles are partially sintered at 700 °C, forming nearly a glass foam cell structure with smaller size cells on the cell edges (Fig. 11(b)). As the sintering temperature increases to 725 °C, a typical glass foam cell structure starts to appear (Fig. 11(c)). At 750 °C, a completely dense glass foam cell-wall structure is observed (Fig. 11(d)). Note also that the small size cells seen on the cell wall edges increase when the sintering temperature increases from 725 to 750 °C (Fig. 11(c) and (d)), resulting from the increased rate of the thermonitrite decomposition as the sintering temperature increases.

Finally, the present geopolymer and glass foam processing methods are also comparable with the light-weight concrete (ALC) and glass foam processing. In ALC, a slurry of silica, Portland cement, lime, and water is foamed using an Al foaming agent. The foamed green body is then strengthened by autoclaving with the formation of tobermorite and crystallized C-S-H as the main binding phases. The formation of the phases depends on the bulk CaO/SiO_2 ratio, autoclaving temperature (100–180 °C), and time (2–8 h), and the compressive strength increases

with the formation of more crystalline tobermorite phases [55]. The compressive strength of ALC ranged from 0.64 to 3.14 MPa between 297 and 589 kg m^{-3} [56]. The compressive strengths of the present geopolymer foams are also comparable with those of ALC, ranging from 0.53 to 3 MPa between similar densities. The processing temperatures of conventional glass foams were reported to be 750–950 °C using a $CaCO_3$ foaming agent [22,23] and 950 °C using a SiC foaming agent [24]. A relatively high processing temperature involved is the main reason for the high production cost of glass foams [21]. Contrary to this, the market size of glass foams has been steadily growing in all countries over the past two decades [21] because glass foams are environmentally friendly in their production and utilization [25]. The similarities in the compressive strength and thermal conductivities of the sintered geopolymer foams in the present study with conventionally processed geopolymer foams show an alternative processing method for glass foam processing. With this method, the intricate geometries of geopolymer foam structures can also be processed nearly at room temperature and then sintered at a high temperature to obtain near-net-shape 3D glass
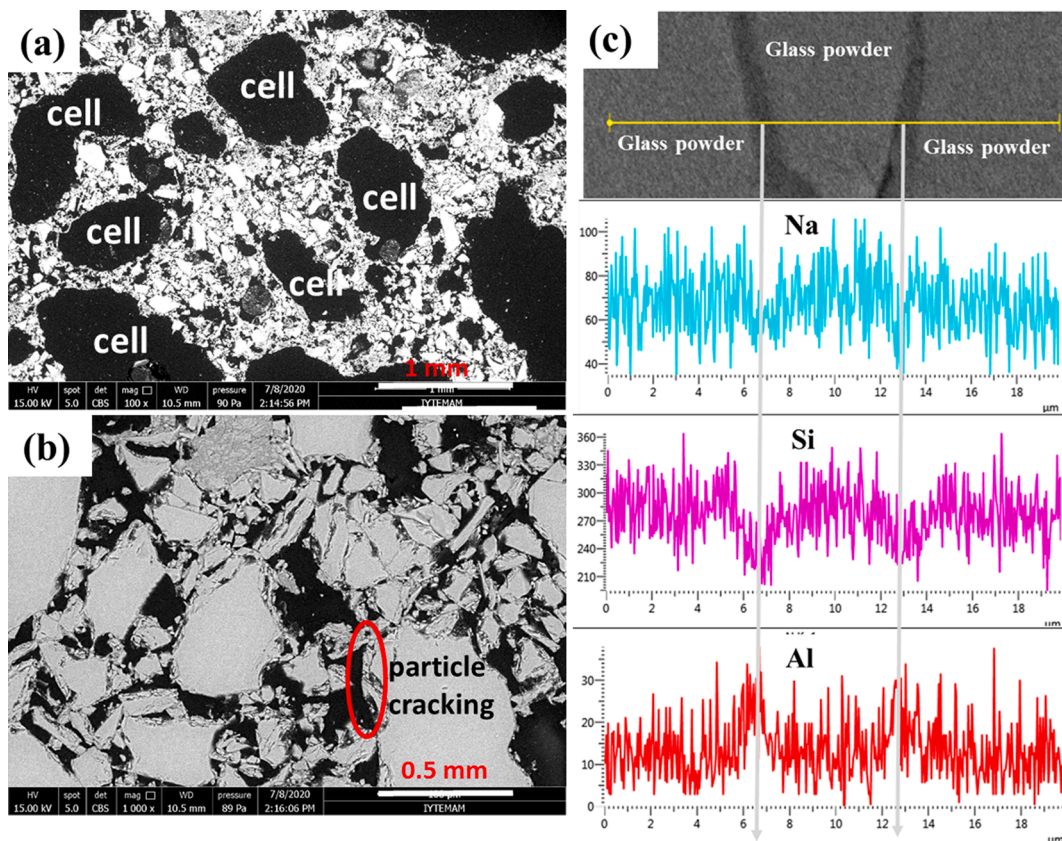
Fig. 10. SEM micrographs of the polished geopolymer foam samples (processed using coarse powder slurries, S/L = 2, and 2 wt% Al) showing (a) the cellular structure and (b) glass particles on the cell walls and (c) the EDX line scan analysis.
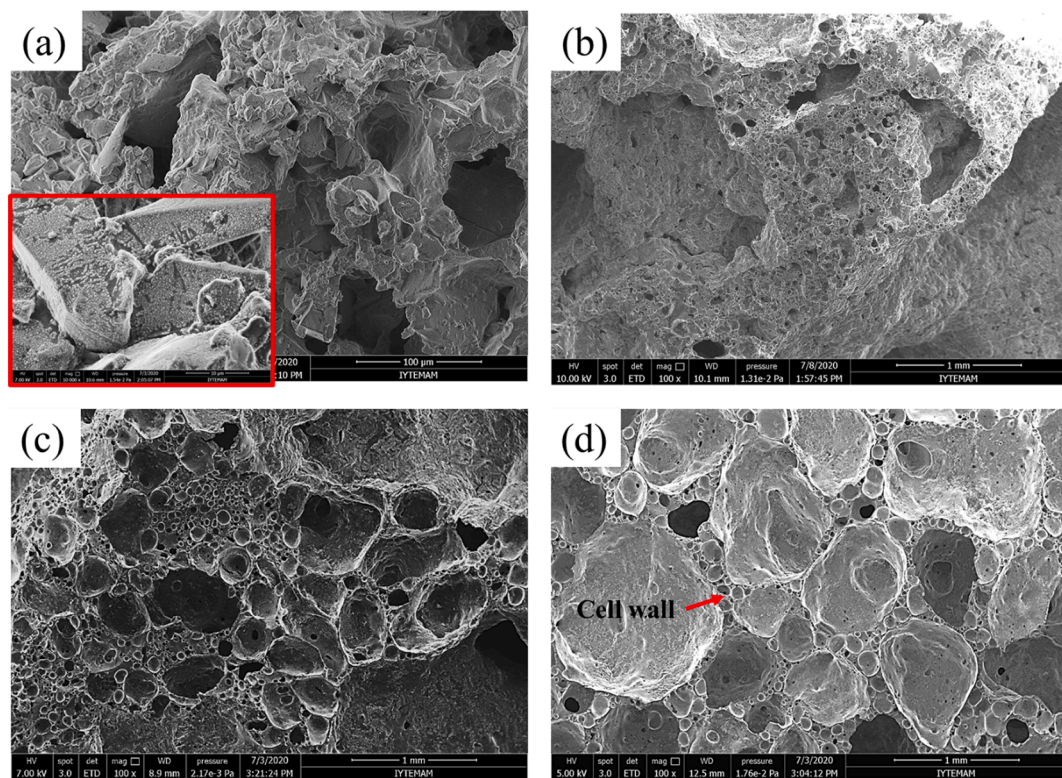

Fig. 11. SEM images of the fracture surfaces of (a) a geopolymer foam and geopolymer foams sintered at (b) 700, (c) 725, and (d) 750 °C (foams were processed using the coarse powder slurry, S/L = 2, and 2 wt% Al).

foam structures.

4 Conclusions

Geopolymer slurries of WG powders were foamed in order to determine their expansion behaviors. The resultant geopolymer foams were sintered at 600, 700, 725, and 750 °C. The following were concluded:

1) The expansion and temperature of the slurries with a low S/L ratio and Al wt% were shown to be limited by the amount of Al added. The Al powder completely reacted with water, leading to relatively lower expansions and temperatures in these slurries.

2) The temperature of the slurries with a higher S/L ratio and Al wt% increased up to a saturation point, 85–88 °C. The rise of the slurry temperature increased both the geopolymerization reaction rate and the S/L ratios of the slurries (due to the rapid liquid evaporation). The resultant increase in the apparent viscosities finally ended up with the termination (solidification) of the slurry expansions. At a very high S/L ratio and Al wt%, the excessive increase in the slurry viscosities caused a reduction in the expansions.

3) In the sintered geopolymer foams, the partial melting of the glass particles started after about 700 °C, and sintering above this temperature resulted in a reduction in the final foam density due to the release of CO_2 gas by the decomposition of thermonitrite.

4) The similar compressive strengths and thermal conductivities of the sintered geopolymer foams in the present study with those of conventionally processed geopolymer foams open an alternative route for glass foam processing. The route is proposed to construct the 3D near-net-shape glass foam structures by applying a shaping process at a low temperature and a sintering process at a high temperature.

CRediT authorship contribution statement

Dilan Polat: Investigation, Formal analysis. **Mustafa Güden:** Conceptualization, Writing - review & editing, Supervision.

Declaration of Competing Interest

The authors declare that they have no known competing financial interests or personal relationships that could have appeared to influence the work reported in this paper.

References

[1] J. Davidovits, GEOPOLYMERS Inorganic polymerie new materials, J. Therm. Anal. Calorim. 37 (8) (1991) 1633–1656.

[2] P. Zhang, K. Wang, Q. Li, J. Wang, Y. Ling, Fabrication and engineering properties of concretes based on geopolymers/alkali-activated binders - A review, J. Cleaner Prod. 258 (2020), 120896.

[3] R.M. Novais, G. Ascensão, N. Ferreira, M.P. Seabra, J.A. Labrincha, Influence of water and aluminium powder content on the properties of waste-containing geopolymer foams, Ceram. Int. 44 (6) (2018) 6242–6249.

[4] J.G. Sanjayan, A. Nazari, L. Chen, G.H. Nguyen, Physical and mechanical properties of lightweight aerated geopolymer, Constr. Build. Mater. 79 (2015) 236–244.

[5] S. Petlitckaia, A. Poulesquen, Design of lightweight metakaolin based geopolymer foamed with hydrogen peroxide, Ceram. Int. 45 (1) (2019) 1322–1330.

[6] J.L.P.a.J.S.J.v. Deventer, Geopolymers: Structure, processing, properties and industrial applications, Woodhead Publishing Limited and CRC Press LLC, Woodhead Publishing Limited, Abington Hall, Granta Park, Great Abington, Cambridge CB21 6AH, UK, 2009.

[7] Z. Zhang, J.L. Provis, A. Reid, H. Wang, Geopolymer foam concrete: an emerging material for sustainable construction, Constr. Build. Mater. 56 (2014) 113–127.

[8] V. Ducman, L. Korat, Characterization of geopolymer fly-ash based foams obtained with the addition of Al powder or H2O2 as foaming agents, Mater. Charact. 113 (2016) 207–213.

[9] A. Hajimohammadi, T. Ngo, P. Mendis, J. Sanjayan, Regulating the chemical foaming reaction to control the porosity of geopolymer foams, Mater. Des. 120 (2017) 255–265.

[10] C. Leiva, Y. Luna-Galiano, C. Arenas, B. Alonso-Fariñas, C. Fernández-Pereira, A porous geopolymer based on aluminum-waste with acoustic properties, Waste Manage. 95 (2019) 504–512.

[11] D. Eliche-Quesada, S. Ruiz-Molina, L. Pérez-Villarejo, E. Castro, P.J. Sánchez-Soto, Dust filter of secondary aluminium industry as raw material of geopolymer foams, J. Build. Eng. 32 (2020), 101656.

[12] D. Belitskus, Reaction of aluminum with sodium hydroxide solution as a source of hydrogen, J. Electrochem. Soc. 117 (8) (1970) 1097, https://doi.org/10.1149/1.2407730.

[13] T. Hiraki, M. Takeuchi, M. Hisa, T. Akiyama, Hydrogen production from waste aluminum at different temperatures, with LCA, Mater. Trans. 46 (5) (2005) 1052–1057.

[14] S.S. Martínez, W. López Benítes, A.A. Álvarez Gallegos, P.J. Sebastián, Recycling of aluminum to produce green energy, Sol. Energy Mater. Sol. Cells 88 (2) (2005) 237–243.

[15] A. Hajimohammadi, T. Ngo, P. Mendis, How does aluminium foaming agent impact the geopolymer formation mechanism? Cem. Concr. Compos. 80 (2017) 277–286.

[16] R.M. Novais, G. Ascensão, M.P. Seabra, J.A. Labrincha, Waste glass from end-of-life fluorescent lamps as raw material in geopolymers, Waste Manage. 52 (2016) 245–255.

[17] R. Si, Q. Dai, S. Guo, J. Wang, Mechanical property, nanopore structure and drying shrinkage of metakaolin-based geopolymer with waste glass powder, J. Cleaner Prod. 242 (2020), 118502.

[18] R. Xiao, Y. Ma, X. Jiang, M. Zhang, Y. Zhang, Y. Wang, B. Huang, Q. He, Strength, microstructure, efflorescence behavior and environmental impacts of waste glass geopolymers cured at ambient temperature, J. Cleaner Prod. 252 (2020), 119610.

[19] C. Bai, H. Li, E. Bernardo, P. Colombo, Waste-to-resource preparation of glass-containing foams from geopolymers, Ceram. Int. 45 (6) (2019) 7196–7202.

[20] G. Kastiukas, X. Zhou, K.T. Wan, J.J.J.o.M.i.C.E. Castro Gomes, Lightweight alkali-activated material from mining and glass waste by chemical and physical foaming, 31(3) (2018) 04018397.

[21] Y. Attila, M. Güden, A. Taşdemirci, Foam glass processing using a polishing glass powder residue, Ceram. Int. 39 (5) (2013) 5869–5877.

[22] D. Zeren, U. Şentürk, M. Güden, The expansion behavior of slurries containing recycled glass powder carboxymethyl cellulose, lime and aluminum powder, Constr. Build. Mater. 240 (2020), 117898.

[23] C. Koerner, in: Engineering MaterialsIntegral Foam Molding of Light Metals, Springer Berlin Heidelberg, Berlin, Heidelberg, 2008, pp. 77–102, https://doi.org/10.1007/978-3-540-68839-6_4.

[24] A. Daoud, Effect of fly ash addition on the structure and compressive properties of 4032–fly ash particle composite foams, J. Alloy. Compd. 487 (1-2) (2009) 618–625.

[25] B.J. Konijn, O.B.J. Sanderink, N.P. Kruyt, Experimental study of the viscosity of suspensions: Effect of solid fraction, particle size and suspending liquid, Powder Technol. 266 (2014) 61–69.

[26] E.R. Andersen, E.J. Andersen, Method for producing hydrogen, Google Patents (2003).

[27] S.E. Abo Sawan, M.F. Zawrah, R.M. Khattab, A.A. Abdel-Shafi, In-situ formation of geopolymer foams through addition of silica fume: Preparation and sinterability, Mater. Chem. Phys. 239 (2020) 121998, https://doi.org/10.1016/j.matchemphys.2019.121998.

[28] L.J. Gibson, M.F. Ashby, Cellular Solids: Structure and Properties, 2 ed., Cambridge University Press, Cambridge, 1997.

[29] E. Bernardo, R. Cedro, M. Florean, S. Hreglich, Reutilization and stabilization of wastes by the production of glass foams, Ceram. Int. 33 (6) (2007) 963–968.

[30] L. Dembovska, D. Bajare, V. Ducman, L. Korat, G. Bumanis, The use of different by-products in the production of lightweight alkali activated building materials, Constr. Build. Mater. 135 (2017) 315–322.

[31] Wrap, www.wrap.org.uk, 2011.

[32] H.R. Fernandes, D.U. Tulyaganov, J.M.F. Ferreira, Production and characterisation of glass ceramic foams from recycled raw materials, Adv. Appl. Ceram. 108 (1) (2009) 9–13.

[33] J.P. Wu, A.R. Boccaccini, P.D. Lee, M.J. Kershaw, R.D. Rawlings, Glass ceramic foams from coal ash and waste glass: production and characterisation, Adv. Appl. Ceram. 105 (1) (2006) 32–39.

[34] J. Garcia-Ten, A. Saburit, M.J. Orts, E. Bernardo, P. Colombo, Glass foams from oxidation/reduction reactions using SiC, Si3N4 and AlN powders, Glass Technology-Eur. J. Glass Sci. Technol. Part A 52 (4) (2011) 103–110.

[35] A.S. Llaudis, M.J.O. Tari, F.J.G. Ten, E. Bernardo, P. Colombo, Foaming of flat glass cullet using Si3N4 and MnO2 powders, Ceram. Int. 35 (5) (2009) 1953–1959.

[36] A.I. Shutov, L.I. Yashurkaeva, S.V. Alekseev, T.V. Yashurkaev, Modeling of the structure of heat-insulating foam glass, Glass Ceram. 64 (11-12) (2007) 397–399.

[37] O.V. Kaz'mina, V.I. Vereshchagin, A.N. Abiyaka, Prospects for use of finely disperse quartz sands in production of foam-glass crystalline materials, Glass Ceram. 65 (9-10) (2008) 319–321.

[38] O.V. Kaz'mina, V.I. Vereshchagin, A.N. Abiyaka, Assessment of the compositions and components for obtaining foam-glass-crystalline materials from aluminosilicate initial materials, Glass Ceram. 66 (3-4) (2009) 82–85.

[39] E. Bernardo, G. Scarinci, P. Bertuzzi, P. Ercole, L. Ramon, Recycling of waste glasses into partially crystallized glass foams, J. Porous Mater. 17 (3) (2010) 359–365.

[40] M.S. Garkavi, O.K. Mel'chaeva, A.I. Nazarova, Effect of the process parameters of mix preparation on the properties of foam glass, Glass Ceram. 68 (1-2) (2011) 44–46.

[41] J.G. Bai, X.H. Yang, S.C. Xu, W.J. Jing, J.F. Yang, Preparation of foam glass from waste glass and fly ash, Mater. Lett. 136 (2014) 52–54.

[42] J.L. Bian, W.L. Cao, L. Yang, C.Q. Xiong, Experimental Research on the Mechanical Properties of Tailing Microcrystalline Foam Glass, Materials 11 (10) (2018) 19.

[43] C.P. Xi, F. Zheng, J.H. Xu, W.G. Yang, Y.Q. Peng, Y. Li, P. Li, Q. Zhen, S. Bashir, J. L. Liu, Preparation of glass-ceramic foams using extracted titanium tailing and glass waste as raw materials, Constr. Build. Mater. 190 (2018) 896–909.

[44] B.S. Semukhin, O.V. Kazmina, A.Y. Volkova, V.I. Suslyayev, Physical characteristics of foam glass modified with zirconium dioxide, Russ. Phys. J. 59 (12) (2017) 2130–2136.

[45] W.L. Huo, S. Yan, J.M. Wu, J.J. Liu, Y.G. Chen, Y.N. Qu, X.Y. Tang, J.L. Yang, A novel fabrication method for glass foams with small pore size and controllable pore structure, J. Am. Ceram. Soc. 100 (12) (2017) 5502–5511.

[46] Z. Zhang, J.L. Provis, A. Reid, H. Wang, Mechanical, thermal insulation, thermal resistance and acoustic absorption properties of geopolymer foam concrete, Cem. Concr. Compos. 62 (2015) 97–105.

[47] M.Y.J. Liu, U.J. Alengaram, M.Z. Jumaat, K.H. Mo, Evaluation of thermal conductivity, mechanical and transport properties of lightweight aggregate foamed geopolymer concrete, Energy Build. 72 (2014) 238–245.

[48] L. Senff, R.M. Novais, J. Carvalheiras, J.A. Labrincha, Eco-friendly approach to enhance the mechanical performance of geopolymer foams: Using glass fibre waste coming from wind blade production, Constr. Build. Mater. 239 (2020) 117805, https://doi.org/10.1016/j.conbuildmat.2019.117805.

[49] G. Kastiukas, X. Zhou, K.T. Wan, J.J.J.o.M.i.C.E. Castro Gomes, Lightweight alkali-activated material from mining and glass waste by chemical and physical foaming, 31(3) (2019) 04018397.

[50] F. Méar, P. Yot, R. Viennois, M. Ribes, Mechanical behaviour and thermal and electrical properties of foam glass, Ceram. Int. 33 (4) (2007) 543–550.

[51] N.M. Bobkova, S.E. Barantseva, E.E. Trusova, Production of foam glass with granite siftings from the Mikashevichi deposit, Glass Ceram. 64 (1-2) (2007) 47–50.

[52] J. König, R.R. Petersen, N. Iversen, Y. Yue, Suppressing the effect of cullet composition on the formation and properties of foamed glass, Ceram. Int. 44 (10) (2018) 11143–11150.

[53] C. Finocchiaro, G. Barone, P. Mazzoleni, C. Leonelli, A. Gharzouni, S. Rossignol, FT-IR study of early stages of alkali activated materials based on pyroclastic deposits (Mt. Etna, Sicily, Italy) using two different alkaline solutions, Constr. Build. Mater. 262 (2020) 120095.

[54] M. Torres-Carrasco, J.G. Palomo, F. Puertas, Sodium silicate solutions from dissolution of glasswastes. Statistical analysis, Materiales de Construcción 64 (314) (2014) e014, https://doi.org/10.3989/mc.2014.v64.i31410.3989/mc.2014.05213.

[55] X. Qu, X. Zhao, Previous and present investigations on the components, microstructure and main properties of autoclaved aerated concrete – A review, Constr. Build. Mater. 135 (2017) 505–516.

[56] Ivailo Petrov, Ernst Schlegel, Application of automatic image analysis for the investigation of autoclaved aerated concrete structure, Cem. Concr. Res. 24 (5) (1994) 830–840.